

THE MHD COLLAPSAR MODEL FOR GRBS: AN INFLOW PRODUCES AN OUTFLOW

D. Proga ¹

RESUMEN

El resumen será traducido al español por los editores. We present our recent results from numerical simulations of a magnetized flow in the vicinity of a black hole in the context of the collapsar model for GRBs. The simulations show that after an initial transient, the flow settles into a complex convolution of several distinct, time-dependent flow components including an accretion torus, its corona and outflow, an inflow and an outflow in the polar funnel. We focus on studying the nature and connection between these components, in particular between the inflows and related outflows. We find that rotational and MHD effects launch, accelerate, and sustain the outflows. We also find that an outflow can be formed even when the collapsing envelope has initially a very weak magnetic field and a very small angular momentum. Our main conclusion is that even for a relatively weak initial magnetic field and a slow rotation, a gravitational collapse of a stellar envelope can lead to formation of a very strong and very fast jet.

ABSTRACT

We present our recent results from numerical simulations of a magnetized flow in the vicinity of a black hole in the context of the collapsar model for GRBs. The simulations show that after an initial transient, the flow settles into a complex convolution of several distinct, time-dependent flow components including an accretion torus, its corona and outflow, an inflow and an outflow in the polar funnel. We focus on studying the nature and connection between these components, in particular between the inflows and related outflows. We find that rotational and MHD effects launch, accelerate, and sustain the outflows. We also find that an outflow can be formed even when the collapsing envelope has initially a very weak magnetic field and a very small angular momentum. Our main conclusion is that even for a relatively weak initial magnetic field and a slow rotation, a gravitational collapse of a stellar envelope can lead to formation of a very strong and very fast jet.

Key Words: **ACCRETION, ACCRETION DISKS — GAMMA RAYS: BURSTS — METHODS: NUMERICAL — MHD — STARS: WINDS, OUTFLOWS**

1. INTRODUCTION

Gamma-ray burts (GRBs) are associated with the huge release of energy in a matter of seconds. The collapsar model is one of most promising scenarios to explain these as well as other properties of GRBs (Woosley 1993; Paczyński 1998; MacFadyen & Woosley 1999; Popham, Woosley & Fryer 1999; MacFadyen, Woosley & Heger 2001; Proga et al. 2003). In this scenario, the collapsed iron core of a massive star accretes gas at a high rate ($\sim 1M_{\odot} s^{-1}$) producing a large neutrino flux, a powerful outflow, and a GRB. Many breakthroughs were made in studying GRBs. For example, the association of long duration GRBs with stellar collapse was firmly confirmed (Hjorth et al. 2003, Stanek et al. 2003). Nevertheless, basic properties of the GRB central engine are quite uncertain. This is because the physical conditions in the central engine are extreme and

complex (e.g., gravitational field is very strong, the temperature and the mass and energy densities are very high; large scale supersonic/relativistic flows and small scale turbulent flows are physically connected). Additionally, magnetic fields are most likely very important in determining the properties of the central engine.

Effects of magnetic fields in the context of the collapsar model have been studied by a few groups (e.g., Mizuno, Yamada, Koide, & Shibata 2004; Mizuno, et al. 2004; De Villiers, Staff, & Ouyed 2005). The main focus of these studies is on 2 and 3 dimensional general relativistic magnetohydrodynamic (GR MHD) simulations of jets launched self-consistently from accretion disks orbiting Schwarzschild or Kerr black holes. These are very important studies as they capture a few of the key elements of the central engine and soon may include more elements such as sophisticated equation of state and neutrino physics.

¹Department of Physics, University of Nevada, Las Vegas, USA

Here, we present and discuss results from 2.5-dimensional, magnetohydrodynamic (MHD) simulations of the collapsar model using pseudo-Newtonian potential. These simulations (see also Proga et al. 2003) are an extension of the work of Proga & Begelman (2003, hereafter PB03) who studied MHD accretion flows onto a black hole (BH). In particular, the collapsar simulations include a realistic equation of state, photodisintegration of bound nuclei and cooling due to neutrino emission. The simulations presented here are also an extension of collapsar simulations by MacFadyen & Woosley (1999), as they include very similar neutrino physics and initial conditions but are in the MHD instead hydrodynamical (HD) limit.

2. MODELS

Proga et al.'s simulation begins after the $1.7 M_{\odot}$ iron core of a $25 M_{\odot}$ presupernova star has collapsed and follows the ensuing accretion of the $7 M_{\odot}$ helium envelope onto the central black hole formed by the collapsed iron core. A spherically symmetric progenitor model is assumed, but the symmetry is broken by the introduction of a small, latitude-dependent angular momentum and a weak split-monopole magnetic field. For more details, see Proga et al. (2003). We refer to the model presented in Proga et al. as run A. We will also present results from model B which is a rerun of model A with the numerical resolution increased by a factor of 2 in the latitudinal direction (see section 3.2). Run B has also a higher resolution in the radial direction compared to run A; the resolution increase is a function of radius and is of a factor of 19 at the smallest radii and of a factor of 1.015 at the largest radii. Run B differs also from run A in the way we set up the initial conditions. However, despite these differences the gross properties of the solution during the later phase of the evolution are very similar for both runs. The details of run B are in Proga (2005; in preparation).

3. RESULTS

3.1. *Fiducial run*

Figure 1 shows time sequence of logarithmic density (top) and toroidal magnetic field maps (bottom) overplotted with the direction of the poloidal velocity from run A during the early phase of the evolution. The figure illustrates how after a transient episode of infall, lasting about 0.13 s, the gas with $l \approx 2R_{SC}$ starts to pile up outside the black hole and to form a thick torus bounded by a centrifugal barrier near the rotation axis. Soon after the torus forms (i.e., within a couple of orbital times at the inner edge),

the magnetic field is amplified by shear and the magnetorotational instability (MRI, e.g., Balbus & Hawley 1991). We note that the third possible mechanism to increase the magnetic field, compression is negligible here because the initial field as well as the infalling gas are radial (e.g., see the top right panel in Fig. 2). The fast growth of the magnetic fields is exemplified by the growth of the toroidal field as shown in the bottom row of panels in Fig. 1. We have verified that most of the inner torus is unstable to MRI, and that our simulations have enough resolution to resolve, albeit marginally, the fastest growing MRI mode (see also Section 3.2 for the presentation of the results from run B).

The magnetic field effects drive the time evolution of the torus including the mass accretion onto a BH. Another important effect of magnetic fields is that the torus produces a magnetized corona and an outflow (e.g., the middle panels in Fig. 1). The presence of the corona and outflow is essential to the evolution of the inner flow at all times and the entire flow close to the rotational axis during the latter phase of the evolution. The outflow very quickly becomes sufficiently strong to overcome supersonically infalling gas (the radial Mach number in the polar funnel near the inner radius is ~ 5) and makes its way outward, reaching the outer boundary at $t = 0.25$ s (see below and fig. 3). Due to limited computing time, run A was stopped at $t = 0.28215$ s, which corresponds to 6705 orbits of the flow near the inner boundary. We expect the accretion to continue much longer, roughly the collapse timescale of the Helium envelope (~ 10 s), as in MacFadyen & Woosley (1999).

Figure 2 shows the time evolution of several gross properties run A: the mass accretion rate through the inner boundary (top left panel), total magnetic energy (top right panel), neutrino luminosity (bottom left panel) and radial Poynting and kinetic flux along the polar axis at $r = 190 R_S$ (bottom right panel). Unless otherwise stated, all quantities in this paper are in cgs units.

Initially, during a precollapse phase, \dot{M}_a stays nearly constant at the level of $\sim 5 \times 10^{32} \text{ g s}^{-1}$. During this phase the zero- l gas inside the initial helium envelope is accreted. Around $t = 0.13$ s, \dot{M}_a rises sharply as the gas from the initial helium envelope reaches the inner boundary. However, this gas has non-zero l and a rotational supported torus and its corona and outflow form (as illustrated in Fig. 1), causing a drop in \dot{M}_a after it reaches a maximum of $2 \times 10^{33} \text{ g s}^{-1}$ at $t = 0.145$ s.

The accretion rate reaches a minimum of $6 \times$

10^{31} g s^{-1} at $t \approx 0.182 \text{ s}$ and then fluctuates with a clear long-term increase. This increase is caused by the contribution from gas with $l < 2R_S c$, which is directly accreted (without need to transport l) from outside the main body of the torus (flow component C in Fig. 4 exemplifies a low l inflow outside the torus). The total mass and angular momentum accreted onto the BH during run A (0.3 s) are $0.1 M_\odot$ and $3 \times 10^{39} \text{ g cm}^2 \text{ s}^{-1}$, respectively.

The top left panel of Fig. 2 shows the time evolution of the total magnetic energy (integrated over the entire computational domain). The late phase of the time evolution of the magnetic energy is characteristic of weakly magnetized rotating accretion flows. Most of the magnetic energy is due to the toroidal component of the field. We note a huge increase of the toroidal magnetic field coinciding with the formation and development of the torus. Both B_ϕ and B_θ are practically zero while B_r is constant during the precollapse phase of the evolution. But at $t = 0.14 \text{ s}$ the total energy in B_ϕ equals that in B_r and just 0.025 s later the B_ϕ energy is higher than the B_r energy by a factor of 50. At the end of simulations the total kinetic energy from the radial, latitudinal and rotational motion are 4×10^{50} , 6.5×10^{49} , and $2.3 \times 10^{51} \text{ erg}$, respectively. These gross properties indicate that the magnetic energy is large enough to play an important role in the flow dynamics.

The bottom left panel of Fig. 2 shows the time evolution of the neutrino luminosity, L_ν . The neutrino luminosity was computed under the assumption that all the gas in the model is optically thin to neutrinos. The neutrino emission stays at a relatively constant level of $3 \times 10^{52} \text{ erg s}^{-1}$ after the torus forms. This indicates that the gross properties – such as the temperature, density, and total mass – of the densest and hottest parts of the flow (the torus) also stay constant during the late phase of the evolution.

The bottom right panel in Fig. 2 shows the area-integrated radial fluxes of magnetic and kinetic energy at $r = 190 R_S$ inside the polar outflow. Formally, the polar outflow is defined as the region where $v_r > 0$ and $\beta < 1$. The Poynting fluxes, stays nearly constant at the level of $\sim 1 \times 10^{51} \text{ egr s}^{-1}$ between $t = 0.185 \text{ s}$ (the time when the jet reached the radius of $190 R_S$) and $t = 0.22 \text{ s}$ then fluctuates with a clear long-term decrease. Comparing the two fluxes, we conclude that the outflow is Poynting flux-dominated, with the Poynting flux exceeding the kinetic energy flux by up to an order of magnitude. We note that the radial fluxes continue to vary with time

by a factor up to 10 even during the late phase of the evolution and they are anti-correlated with the mass accretion. (The radial fluxes show much less detail compared to other properties shown in Fig. 2 because there were computed less frequently during the course of the simulation.)

The decrease of the radial fluxes and their anti-correlation with \dot{M}_A is quite a surprising result because the jet is supposed to be powered by accretion! However, the situation in a collapsing star is complex because \dot{M}_a has two sources: (i) an accretion disk which does power a strong jet and (ii) the low l gas that accretes directly onto a BH and can prevent development of the torus jet. This infalling gas can produce an outflow/jet of its own but with properties different from those of the torus jet (see below).

Figure 3 shows maps of the flow pattern and maps of B_ϕ on four different length scales at $t = 0.285 \text{ s}$ (the left panels show the inner most part of the flow whereas the right panels show the flow on the largest scale). The main outflow is magnetically driven from the torus. Soon after the torus forms, the magnetic field very quickly deviates from its initial radial configuration due to MRI and shear (see Fig. 2). This leads to fast growth of the toroidal magnetic field as field lines wind up due to the differential rotation. As a result the toroidal field dominates over the poloidal field and the gradient of the former drives an outflow.

A comparison between the density and B_ϕ maps shows that the polar regions of low density and high B_ϕ coincide with the region of an outflow. Proga et al. (2003) noted that during the latter phase of the evolution not all of the material in the outflow originated in the innermost part of the torus – a significant part of the outflow is “peeled off” the infalling gas at large radii by the magnetic pressure. However, as our later analysis and simulations show the outflow from the infalling gas is caused not only by the peeling off effect but it is also produced by the magnetic and thermal effects operating inside the infalling gas itself. Thus there are not two but three types of outflows from a collapsing star (see Fig. 4).

The first two panels of the left hand side of Fig. 3 illustrate that the inner torus and its corona and outflow cannot always prevent the low- l gas from reaching the BH. Even the magnetic field cannot do it if the density of the incoming gas is too high (compare the upper and lower halves of the panels in Figs 3 and 5).

We finish the presentation of the results from run A with an analysis of the properties of the ac-

cretion torus, i.e., the main engine in the model. Figure 4 shows the radial profiles of several quantities in run A, angle-averaged over a small wedge near the equator (between $\theta = 86^\circ$ and 94°), and time-averaged over 50 data files covering a period at the end of the simulations (from 0.2629 s through 0.2818 s). We indicate the location of the last stable circular orbit by the vertical dotted line in each panel.

We measure the Reynolds stress, $\alpha_{gas} \equiv \langle \rho v_r \delta v_\phi \rangle / P$, and the Maxwell stress normalized to the magnetic pressure, $\alpha_{mag} \equiv \langle 2B_r B_\phi / B^2 \rangle$. Note that Fig. 4 shows only the magnitude, not the sign, of the normalized stresses. We find that except for $r \lesssim 2.5R_S$ and $10R_S \lesssim r \lesssim 12R_S$, the Maxwell stress dominates over the Reynolds stress in the inner flow. The last panel in Fig. 4 shows that the toroidal component of the magnetic field is dominant for $r < 50 R_S$.

Proga et al.'s simulation explored a relatively conservative case as they allowed for neutrino emission but did not allow for the emitted neutrinos to interact with the gas or annihilate. The only sources of nonadiabatic heating in their simulation are the artificial viscosity and resistivity.

3.2. High resolution run

To explore the nature of the multicomponent flow resulting from a collapse of a rotating star we rerun model A using higher numerical resolution [see Section 3.1 and Proga (2005 in preparation)]. Higher resolution simulations are especially required to study the evolution and effects of MRI. Run B is qualitatively consistent with the results from the fiducial model. In particular, all the flow components found in run A can be also found in run B. Additionally, the properties of the flow components found in run A are consistent with those in run B. For example, MRI drives the evolution of the equatorial torus and the simulations resolve the fastest growing MRI mode.

Figure 5 shows the inner most part of the flow in run B at $t=0.582$ s. The seven main flow components are marked with upper case letters (see the figure caption).

In the context of GRBs, the most important component of the flow is an outflow. The biggest difference between the MHD collapsar model and the HD collapsar model considered by MacFadyen Woosley (1999) is that in the MHD limit, the outflow that develops soon after a torus forms is so strong that it breaks through a star even when very little of a low l gas is accreted whereas in the HD limit, a torus

wind is relatively weak and the polar funnel must be evacuated if the wind were to leave the star.

3.3. An outflow from a very l infall

Generally, runs A and B show that large-scale magnetic fields can produce two types of outflows: (1) a jet from a rotationally supported accretion disk or torus and (2) an outflow from extremely low angular momentum gas that almost radially accretes onto a BH (e.g., PB03, Proga et al. 2003). Both analytic and numerical studies support the view that the former is robust. (e.g., Blandford & Payne 1982; Blandford 1990; De Villier et al. 2003). In fact, most MHD simulations of an accretion disk or torus show outflows (e.g., Uchida & Shibata 1985; Stone & Norman 1994; Hawley & Balbus 2002; De Villier et al. 2004; Mizuno et al. 2004; Kato et al. 2004; McKinney & Gammie 2004). However, the latter which is a simple, self-consistent solution for the MHD jet problem, has not been studied much. To articulate the basic physics that occurs in jet production, Proga (2005) performed simulations of a flow with angular momentum so low that, if not for the effects of MHD, the flow would accrete directly onto a BH without forming a disk. These simulations used simplified physics (i.e., no neutrino cooling and an adiabatic equation of state) similar to that explored by PB03.

In Proga (2005), we found that even with a very weak initial magnetic field, the flow settles into a configuration with four components: (i) an equatorial inflow, (ii) a bipolar outflow, (iii) a polar funnel outflow, and (iv) a polar funnel inflow. The second flow component of the MHD flow represents a simple yet robust example of a well-organized inflow/outflow solution to the problem of MHD jet formation (see Fig. 6) and is the same in nature as components C and B in run B as well as in run A (e.g., Fig. 5). The outflow from the low l infall is heavy, highly magnetized, and driven by magnetic and centrifugal forces. A significant fraction of the total energy in the jet is carried out by a large scale magnetic field. The properties of this outflow help to understand that the time evolution of the outflow in run A. As we mentioned in section 3.1, the low l inflow can block or prevent development of the torus jet, the latter being light. The low l inflow produces the outflow that is heavy and although a significant fraction of its total energy is carried out by a large scale magnetic field it is not Poynting flux-dominated, contrary to the torus jet.

A comparison between various simulations including those presented in section 3.1 and 3.2, where specific angular momentum was higher than that as-

sumed in Proga (2005), indicates that the flow components B and C develop for a wide range of the properties of the flow near the equator and near the poles.

4. CONCLUSIONS

Fully 3 dimensional GR MHD simulations are required to capture many of the effects and instabilities of a magnetized fluid in a rotating star collapsing onto a BH. Neutrino physics, a sophisticated equation of state and self-gravity should also be included. However, such full treatment of the MHD collapsar model is beyond reach of the current numerical codes at least for now.

Here we present results from time-dependent two-dimensional MHD simulations of the collapsar model using pseudo-Newtonian potential. The simulations show that: 1) soon after the rotationally supported torus forms, the magnetic field very quickly starts deviating from purely radial due to MRI and shear. This leads to fast growth of the toroidal magnetic field as field lines wind up due to the torus rotation; 2) The toroidal field dominates over the poloidal field and the gradient of the former drives a torus outflow against supersonically accreting gas through the polar funnel; 3) The torus outflow is Poynting flux-dominated; 4) The torus outflow reaches the outer boundary of the computational domain (5×10^8 cm) with an expansion velocity of 0.2 c; 5) The torus outflow is in a form of a relatively narrow jet (when the jet breaks through the outer boundary its half opening angle is 5°); 6) Most of the energy released during the accretion is in neutrinos, $L_\nu = 2 \times 10^{52}$ erg s^{-1} . Neutrino driving will increase the outflow energy (e.g., Fryer & Mészáros 2003 and references therein), but could also increase the mass loading of the outflow if the energy is deposited in the torus. A comparison of the MHD simulations with their HD counterparts show that a strong outflow breaks through a magnetized star much sooner than through a non-magnetized star.

The above conclusions were reached by Proga et al. (2003) and here we confirmed them using a higher resolution simulation. However, we emphasize the fact that the flow settles into a complex convolution of several distinct, time-dependent flow components and the above mentioned torus and its outflow are just two of them. Other flow components include a torus corona and low l flows. A rotationally supported torus and its corona and outflows were extensively studied in the past and remain a focus of many studies. We stress that in the context of the collapsar model, where very low l and high l fluids are

present, the situation is more complex. Therefore, future work, even without neutrino physics or effects of general relativity, is important to explore connection and interaction of all the flow components, and their observational implications.

We acknowledge support from NASA under ATP grant NNG05GB68G and support provided by NASA through grant HST-AR-10305.05-A from the Space Telescope Science Institute, which is operated by the Association of Universities for Research in Astronomy, Inc., under NASA contract NAS5-26555.

REFERENCES

- Balbus, S. A., & Hawley, J. F. 1991, ApJ, 376, 214
 Blandford, R.D., & Payne D.G. 1982, MNRAS, 199, 883
 Blandford, R.D., *Active Galactic Nuclei* (Eds R. Blandford, H. Netzer & L. Woltjer), Berlin: Springer 1990
 De Villiers, J.-P., Hawley J.F., Krolik J.H., Hirose S. 2005, ApJ, 650, 878
 De Villiers, J.-P., Staff, J., Ouyed, R. 2005, ApJ, submitted, (astro-ph/0502225)
 Fryer, C. L., & Mészáros, P. 2003, ApJ, 588, L25
 Hjorth, J., et al. 2003, Nature, 423, 847
 Kato, Y., Mineshige, S., & Shibata, K. 2004, ApJ, 605, 307
 MacFadyen, A., & Woosley, S.E. 1999, ApJ, 524, 262 (MW)
 MacFadyen, A., Woosley, S.E., & Heger A. 2001, ApJ, 550, 410
 McKinney, J.C., & Gammie, C.F. 2004, ApJ, 611, 977
 Mizuno, Y., Yamada, S., Koide, S., & Shibata, K. 2004, ApJ, 606, 395
 Mizuno, Y., et al. 2004, ApJ, 615, 389
 Paczyński, B. 1998, ApJ, 494, L45
 Popham, R., Woosley, S.E., & Fryer, C. 1999, ApJ, 518, 356
 Proga, D. 2005 ApJ, 629, 397
 Proga, D., & Begelman, M.C. 2003 ApJ, 592, 767 (PB03)
 Proga, D., MacFadyen, A. I., Armitage, P. J., & Begelman, M. C. 2003, ApJ, 599, L5
 Stanek, K.Z., et al. 2003, ApJ, 591, L17
 Stone, J.M., & Norman, M.L. 1994, ApJ, 433, 746
 Uchida, Y., & Schibata K. 1985, PASJ, 37, 515
 Woosley, S.E. 1993, ApJ, 405, 273
 Woosley, S. E., & Weaver, T. A. 1995, ApJS, 101, 181

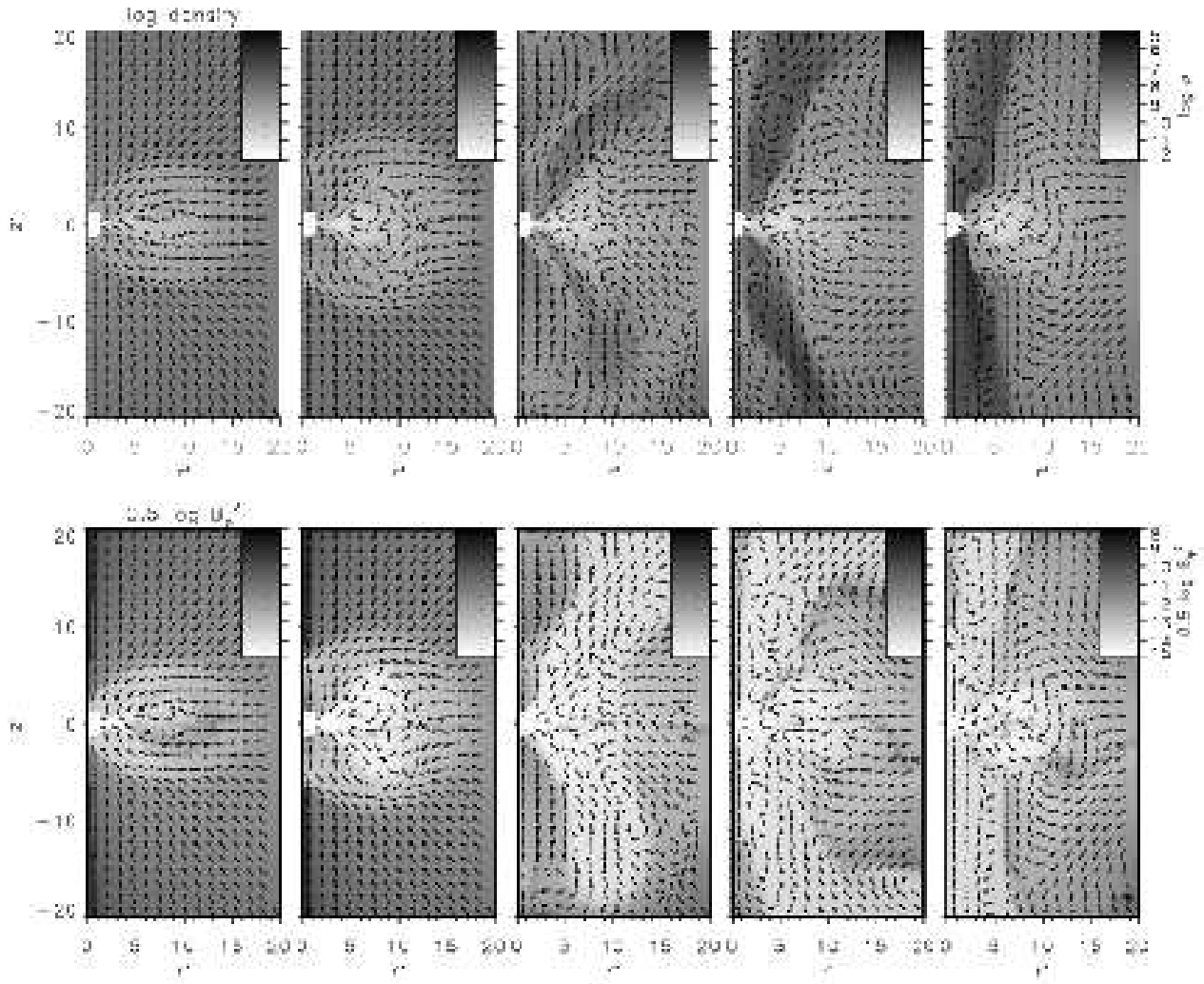


Fig. 1. Sequence of logarithmic density (top) and toroidal magnetic field maps (bottom) overplotted with the direction of the poloidal velocity from run A at times 0.153, 0.161, 0.165, and 0.173 s. The sequence illustrates the early phase of the formation of a rotational supported accretion torus and of a magnetically driven outflow. The length scale is in units of the BH radius (i.e., $r' = r/R_S$ and $z' = z/R_S$).

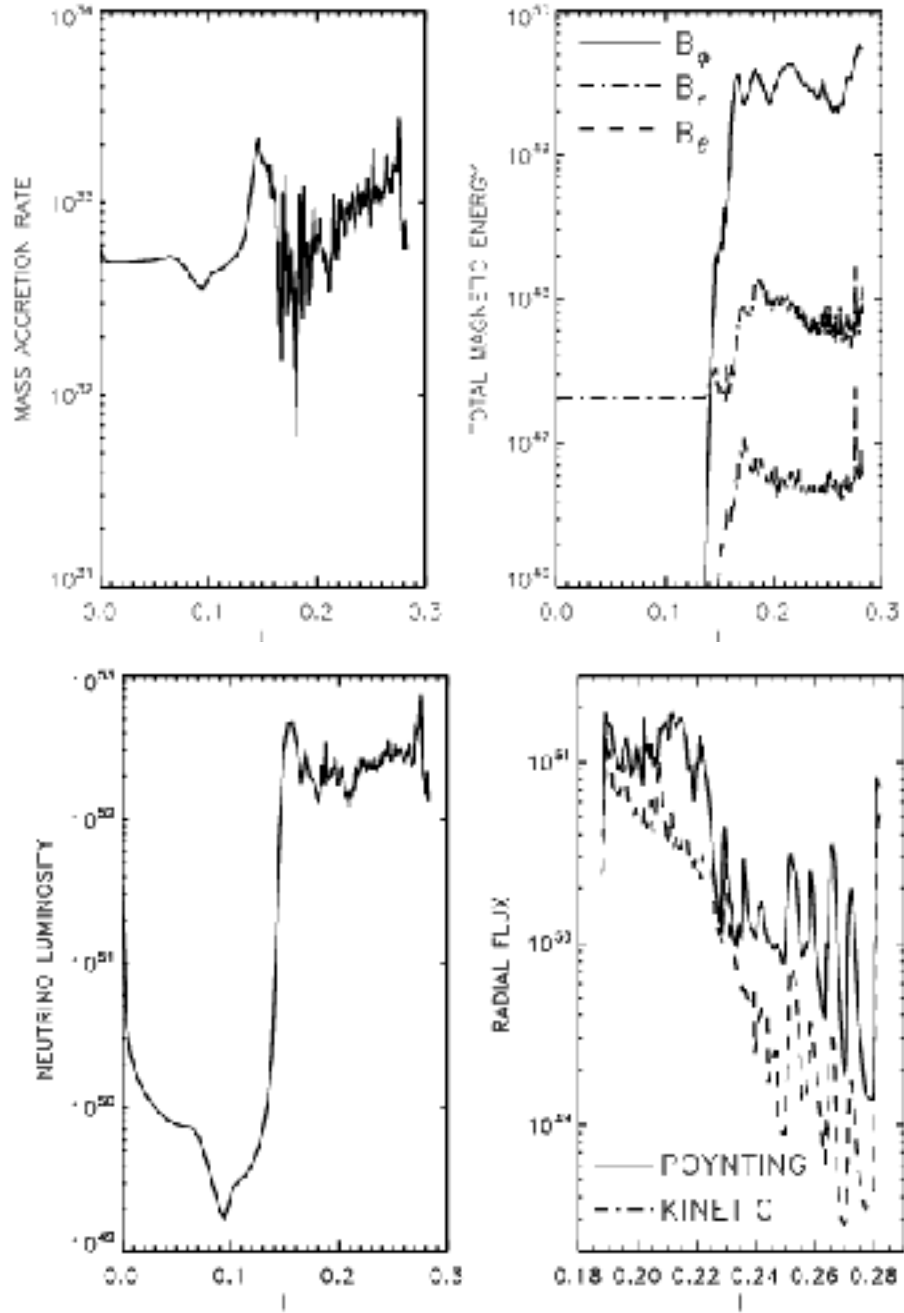


Fig. 2. The time evolution of the mass accretion rate (top left panel), total magnetic energy due to each of the three field components (top right panel), neutrino luminosity (bottom left panel) and area-integrated radial Poynting and kinetic flux in the polar outflow at $r = 190 R_S$ (bottom right panel) for run A. Formally, we define the polar outflow as the region where $v_r > 0$ and $\beta < 1$. Note the difference in the time range in the panel with the radial fluxes.

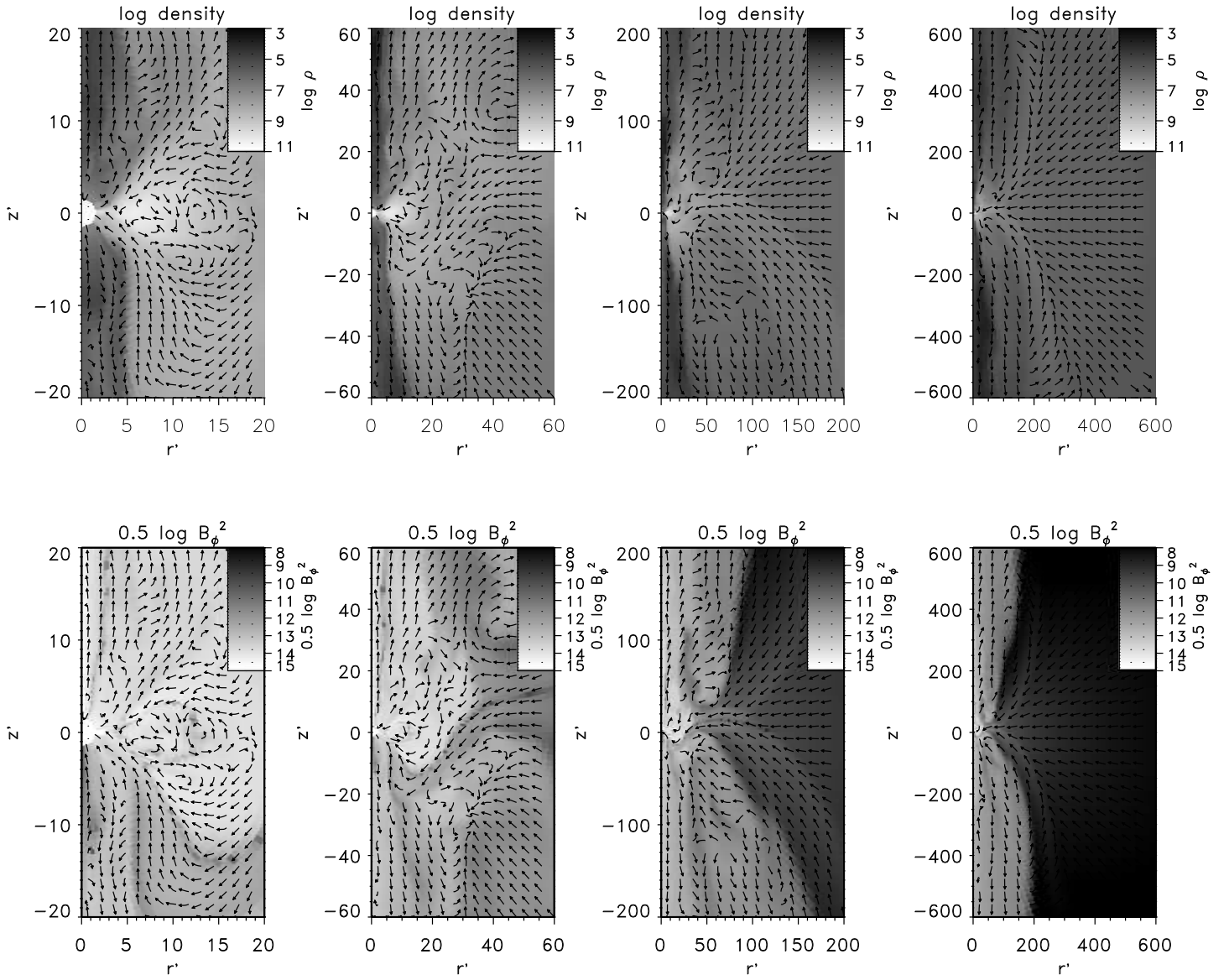


Fig. 3. Maps of logarithmic density (top) and toroidal magnetic field maps (bottom) overplotted with the direction of the poloidal velocity from run A at the end of simulations, i.e. time 0.2815 s. The length range increases from left to the right. Note that the accretion torus is relatively small (it spans from 1 to about $20 R_S$). Nevertheless, this tiny torus generates an outflow and mass and energy that can the dynamics and structure of the collapsing star over a large range of radii along the rotational axis.

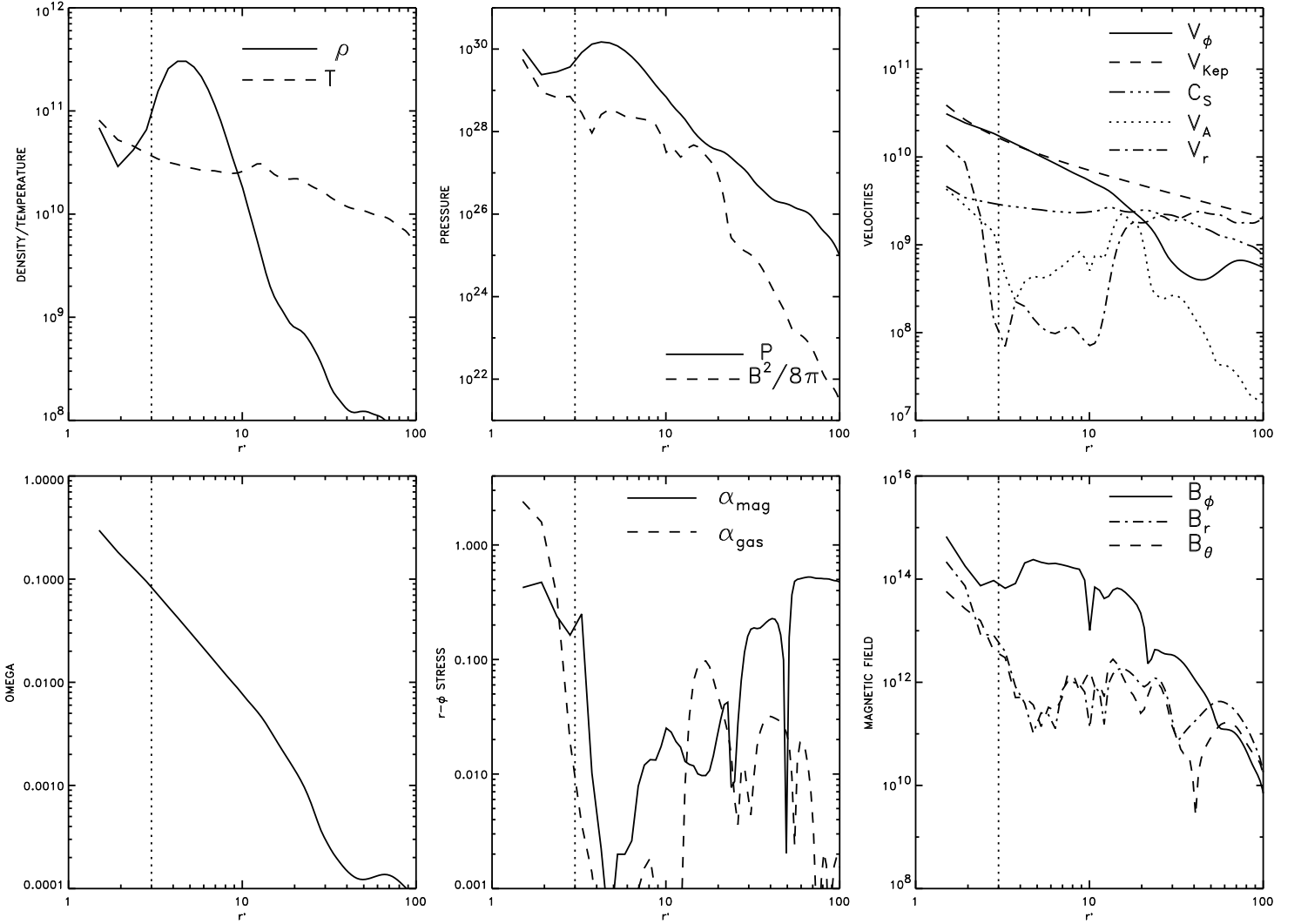


Fig. 4. Radial profiles of various quantities from our run, time-averaged from 0.2629 through 0.2818 s. To construct each plot, we averaged the profiles over angle between $\theta = 86^\circ$ and 94° . The top left panel plots the density (solid line) and temperature (dashed line). The top middle panel plots the gas pressure (solid line) and magnetic pressure. The top right panel plots the rotational, radial, Keplerian, and Alfvén velocities (solid, dashed, dot-dashed, and dotted line, respectively), as well as the sound speed (triple-dot dashed line). The bottom left panel plots the angular velocity in units of $2c/R_s$. The bottom middle panel plots the Maxwell stress, α_{mag} , and the Reynolds stress, α_{gas} (solid and dashed line, respectively). We calculate the Reynolds stress using eq. (15) in PB03 and show only its amplitude. The bottom right panel plots the radial, latitudinal and toroidal components of the magnetic field (dot-dashed, dashed, and solid line, respectively). The length scale is in units of the BH radius (i.e., $r' = r/R_S$).

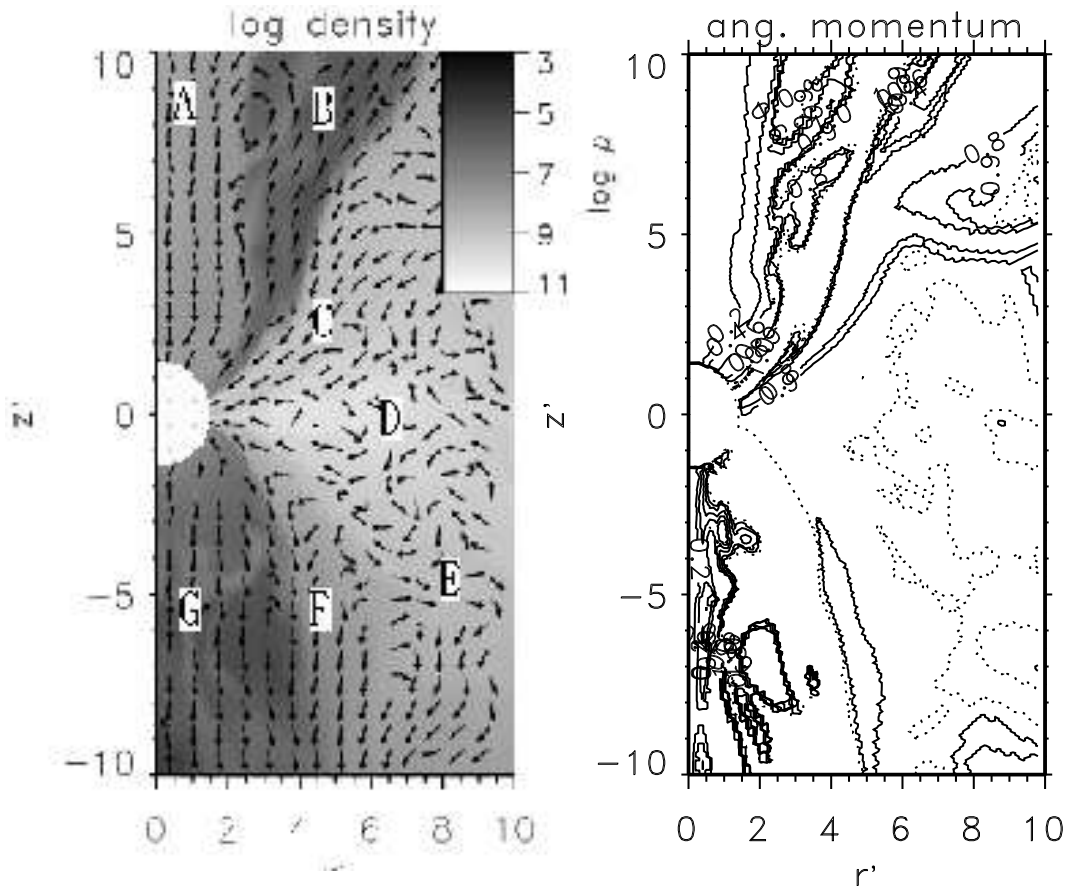


Fig. 5. A map of logarithmic density overplotted with the direction of the poloidal velocity (left panel) and a contour map of specific angular momentum, l (right panel) from high resolution run B at $t = 0.0582$ s. The specific angular momentum is in units of $2R_{Sc}$. The minimum of l (contour closest to the rotational z -axis) is 0.2, and the contour levels are equally spaced at intervals of $l = 0.2$. The maximum of l is 1.0 and its contour is plotted using dotted curves, whereas all the other contours are plotted using solid curves. This figure shows an inner most part of the flow when a torus just formed and started to develop an outflow. Note that the latter pushed aside the polar funnel accretion flow only below the equator. This figure was chosen to illustrate the complexity of the inner most part of the flow inside a collapsing magnetized star. The upper case letters, in the right panel, mark seven major components of this complex flow: A – a very low l polar funnel accretion flow; B – a highly magnetized outflow generated from a low l inflow C; C – an inflow with angular momentum so low that the flow would accrete directly onto a BH; D – a rotationally supported, MHD, turbulent accretion torus; E – a magnetized torus corona; F – a highly magnetized outflow generated from the torus; and G – a polar funnel outflow driven thermally (compare with A). See Proga (2005; in preparation) for more details.

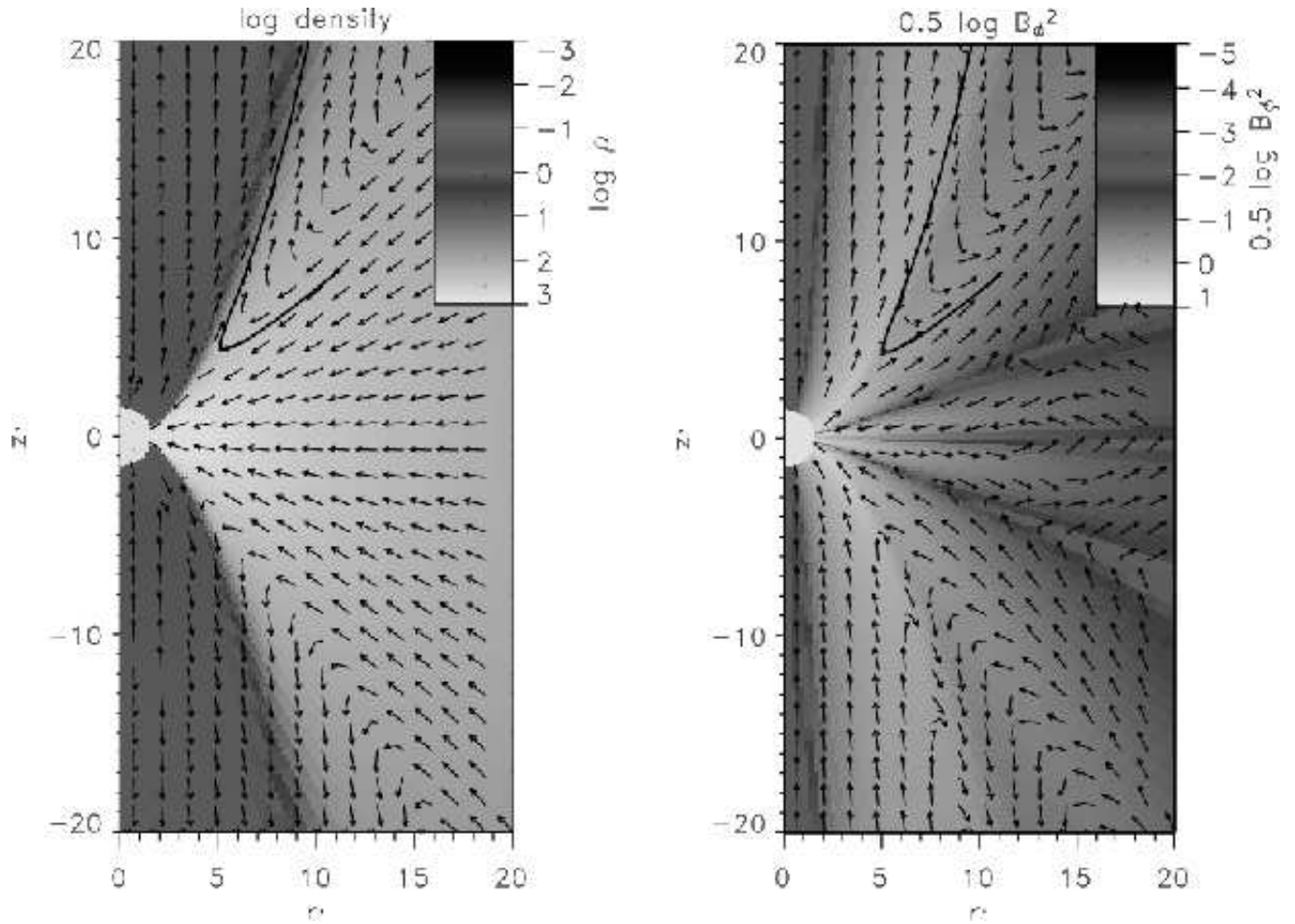


Fig. 6. Maps of logarithmic density (left panel) and toroidal magnetic field (right panel) overplotted with an example of a streamline corresponding to an inflow/outflow for model C. The maps are also overplotted with the direction of the poloidal velocity and the direction of the poloidal field (the left and right panels, respectively). See Proga (2005) for more details.

Daniel Proga; Department of Physics, University of Nevada, 4505 South Maryland Parkway, Las Vegas, NV 89154, USA (dproga@physics.unlv.edu).

This figure "f3da.gif" is available in "gif" format from:

<http://arxiv.org/ps/astro-ph/0512264v1>